SLAC-PUB-235
October 1966

REPORT ON THE STANFORD LINEAR ACCELERATOR CENTER*

G. A. Loew
Stanford Linear Accelerator Center, Stanford, California

In preparing this report, I found myself in somewhat of a dilemma. On the one hand, this is supposed to be a rapporteur talk in which I am to present a status report on the present activities at SLAC. On the other hand, this meeting being an international conference on instrumentation, one might assume that I should concern myself primarily with SLAC instrumentation. Finally, most visitors interested in accelerator physics seem to ask us primarily about our "beam break-up phenomenon" which wiggles the beam up and down along our two miles. What should I talk about?

Right or wrong, I have decided to compromise and attempt to divide my report into three parts. In the first part, after reminding you of some of the main features of our accelerator, I shall try to summarize the present results and performance of the two-mile accelerator. In the second part, I will briefly touch upon some of the main instruments along the machine and the beam switchyard and on how they are tied together in our two control rooms. Finally, I will try to summarize briefly some of the main characteristics of the beam break-up phenomenon and what we intend to do about it.

Figure 1 shows an overall layout of the two-mile accelerator, the beam switchyard, and the end stations. At the beginning, notice the injector; a beam analyzing station at the 40-foot point to examine the beam spectrum and profile before launching; a first so-called "drift section" at the end of the first of 30 sectors; the first beam take-off (not used for the time being); the future location of the first off-axis injector; the positron source in Sector 11; the take-off point for the proposed electron-positron storage ring; the second momentum spectrometer, which presently enables us to run two-thirds of the accelerator when the switchyard is not available; the space for a second off-axis injector; and at the end of the accelerator, the last drift section in Sector 30. At this point the beam switchyard begins with the collimator and the pulsed magnet system which makes it possible to deflect the beam either into End Station A, End Station B, the tune-up dump, or straight ahead into the future End Station C. Also notice the bending magnet systems and the A- and B-beam energy defining slits.

Table I gives a summary of SLAC key dates.

Figure 2 shows a photograph of the accelerator housing. The cross section given in Fig. 3 enables you to see in greater detail the various elements of the accelerator, i.e., the disk-loaded waveguide of which an end-flange is exposed, the rectangular waveguide, the vacuum manifold on the left, the aluminum light pipe which is used for support and alignment of the accelerator, the retractable Fresnel lens which is part of the laser alignment system, and the alignment jacks. Altogether, there are roughly 240 standard and 60 special girders of this type along the machine with their corresponding Fresnel lenses. Figure 4 is a view of the klystron gallery, showing the klystrons with their pulse

*Work supported by the U.S. Atomic Energy Commission.

(Presented at 1966 International Conference on Instrumentation for High Energy Physics, Stanford Linear Accelerator Center, September 9-10, 1966)

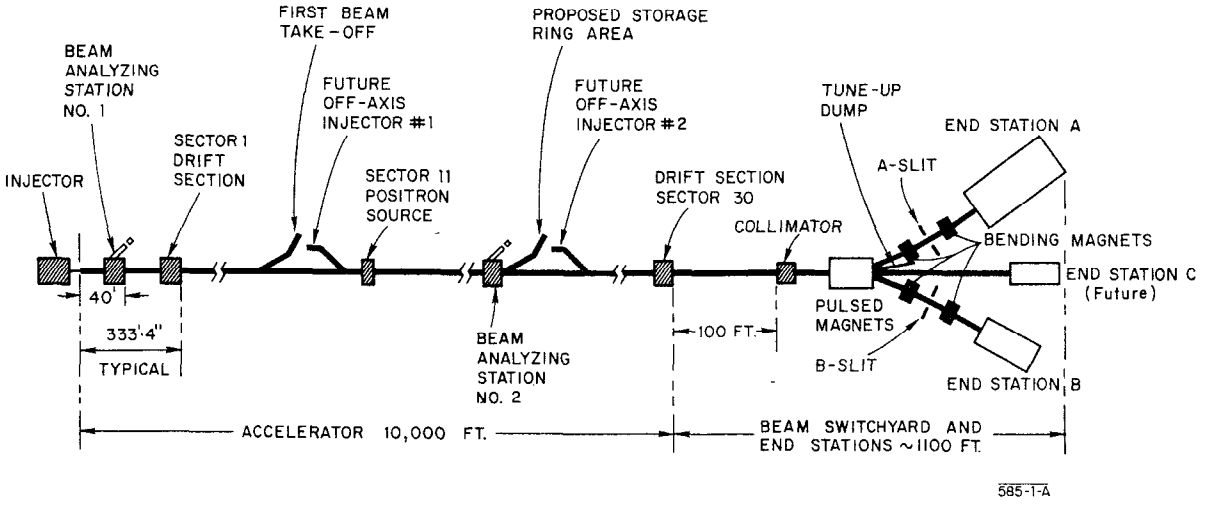

FIG. 1--Overall layout of the two-mile accelerator.

TABLE I

SLAC Key Dates

April, 1957	Proposal for 2-Mile Accelerator
September, 1961	Authorization by Congress
July, 1962	Start of Site Construction
April 21, 1966	Beam to 2/3 Point (Sector 20)
May 21, 1966	Beam Through 30 Sectors to Beam Switchyard
June 2, 1966	18.4 GeV Beam in Beam Switchyard (Tune-up Dump)
July 13, 1966	First 2 GeV Positron Beam (Sector 20)
September, 1966	Beam Planned into End Station A and Beginning of Experiments
October, 1966	Beam Planned into End Station B

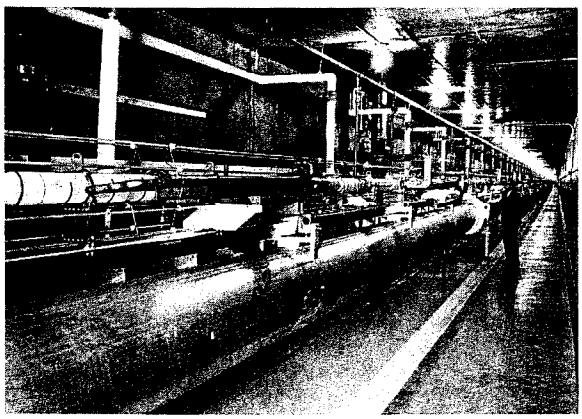

FIG. 2--View of the Accelerator Housing.

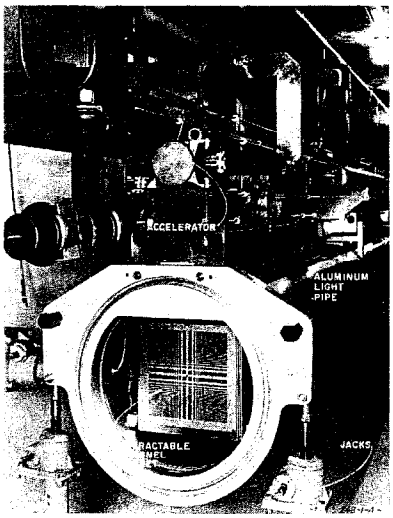

FIG. 3--Accelerator Housing cross section.

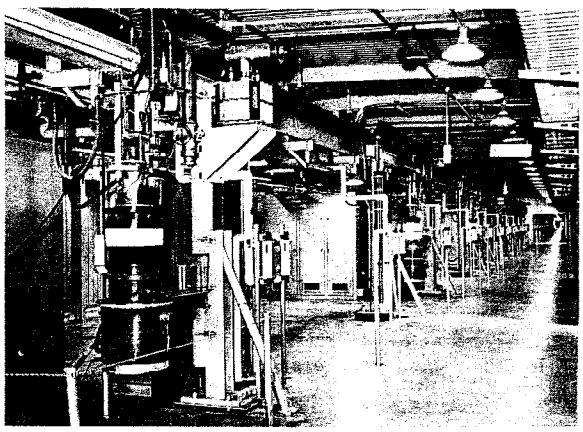

FIG. 4--View of the Klystron Gallery.

transformer tanks, waveguide circuitry, high power modulators, and in the background, their individual control stations. Also, under the roof, notice the vacuum manifold, the insulated rf drive lines, and the vac-ion pumps. Figure 5 is a detailed schematic view of the beam switchyard. Finally, Fig. 6 shows you the present layout of the End Stations. Notice at the top of the drawing, in End Station A, the three spectrometers, the streamer chamber, and the so-called "beam dump east." In End Station B, the future 1-meter bubble chamber and the mu-beam spark chamber are shown. Between these two end stations, a third beam called the C-beam is presently being developed for the Berkeley 80-inch bubble chamber, using the first SLAC rf-separated beam and possibly a neutral beam facility.

Since the electron beam was first turned on in April and May of this year, it has been possible, through numerous machine runs and experiments, to evaluate the actual performance of the accelerator and to compare it with many of the original specifications. Table II summarizes the essential results obtained to date. Notice that the beam break-up effect presently limits the accelerator current to slightly less than half of its specified value.

Now, turning to the general subject of instrumentation, let me present a few figures illustrating instrumentation and controls and how they are centralized and used in the control rooms. Figure 7 shows the layout of a typical drift section, of which there are 30 along the machine. Notice a manual valve at one end and a remote fast-acting valve at the other, the quadrupole "triplet" system which is presently being reconnected as a "doublet" system with the resulting elimination of the large central quadrupole, the steering dipoles, the beam position monitor microwave cavities, the toroid used to monitor beam intensity, a special can into which a beam profile Cerenkov monitor can be inserted, and finally a collimator normally called a beam scraper. In Fig. 8 you can see in greater detail the microwave cavities which constitute the heart of the beam position monitor system and which, through an appropriate phase comparison and beam intensity normalization, enable us to obtain both the horizontal and vertical positions of the beam within less than a millimeter, for a minimum peak current of one milliampere.

The next figures illustrate how this and other instrumentation are used in the Central Control Room. Figure 9 is a photograph of the left-hand side of the Central Control console. In order to simplify operations, this side of the console is reserved primarily for the display of information and control of those functions of the machine having to do with maintenance, i.e., the status of the klystron population, the injector, the switchyard, radiation, vacuum, cooling water, general communications, etc. On this console there are two special panels one of which is shown in Fig. 10. These give direct detailed access to any one of the 30 sectors of the machine. By depressing one of the 30 buttons, the maintenance operator can observe and control the status of each klystron in that sector; he can automatically phase these klystrons, adjust trigger timing and quadrupole current, manually rotate the phase of an entire sector, etc. These observations and actions can be performed without interfering with the main activities taking place on the other side of the Central Control console, shown in Fig. 11. This right-hand side of the console is the domain of the beam operator, sometimes called the beam jockey. Besides

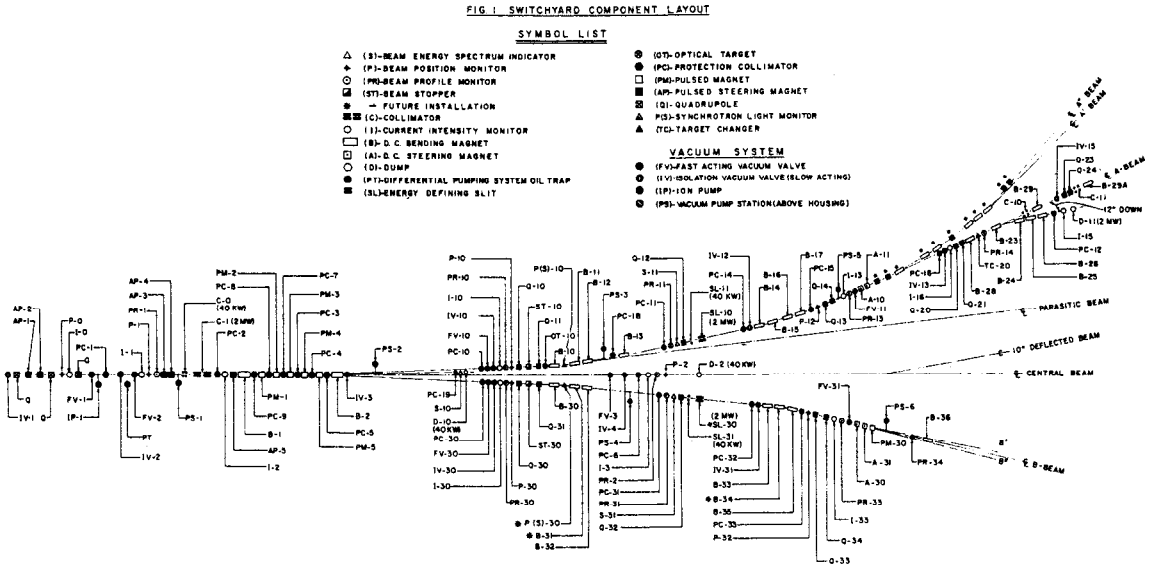

FIG. 5--Beam Switchyard component layout.

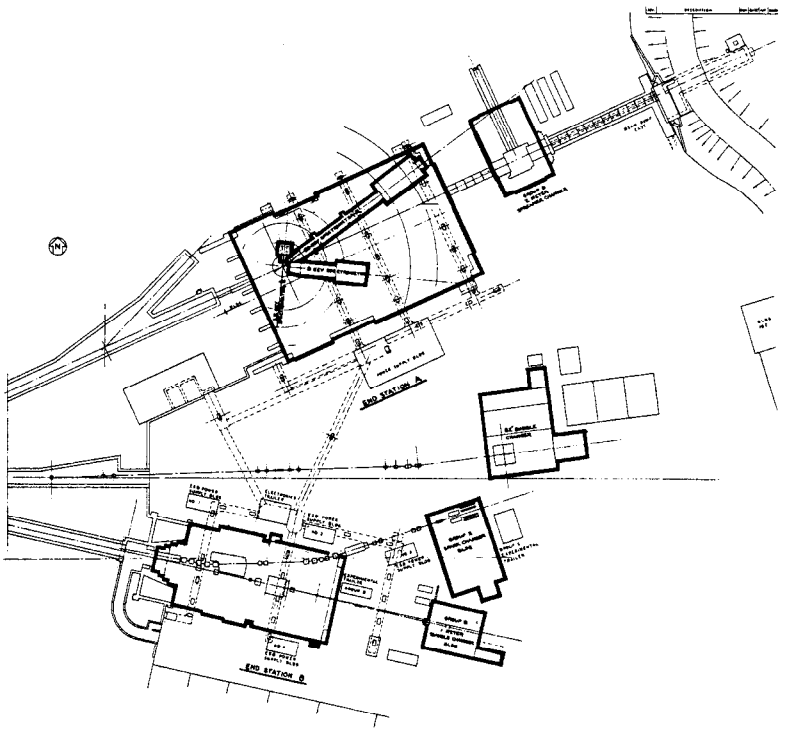

FIG. 6--End Station layout.

TABLE II

COMPARISON OF SIGNIFICANT

SLAC DESIGN PARAMETERS AND PERFORMANCE (September 1966)

	Specified	Actual
Energy contribution per klystron $E_{MeV} = K\sqrt{P_{MW}}$	$K_{max} = 20.6$	$K_{obtained} = 20$ average
Effective[1] number of installed klystrons	242	242
Peak klystron power at 360 pps and 2.5 μsec pulse length	22 MW	22 MW
Conservative[2] klystron peak power at 360 pps		16-18 MW
Maximum beam energy for above conservative level		~ 20 GeV
Maximum peak beam current at 1.6 μsec pulse length	50 mA	20 mA (beam break-up limited)
Corresponding number of e^-/pulse	5×10^{11}	2×10^{11}
Average beam current at 360 pps and 1.6 μsec pulse	~30 μA	~12 μA
Beam loading derivative in GeV/amp	35	35
No. of simultaneous beams at different energies, pulse lengths and repetition rates	3	3
Typical energy spectrum width at half maximum	1%	0.6 - 1.3% depending on total current
Frequency,[3] main drive line (MHz)	476	476
accelerator (MHz)	2856	2856
Range of accuracy of automatic phasing system[4]	$\pm 5^o$	$\pm 5^o$ or better
Electron bunch width at 40 foot point	$< 5^o$	$< 5^o$
Klystron phase stability (within pulse and pulse to pulse)	5^o	5^o
Beam phase space: Injector emittance (mc-cm) ($\pi r \times p_r$)	0.05	0.025
Accelerator emittance (mc-cm)	0.10	0.05
Accelerator vacuum (torr)	$< 10^{-5}$	$\sim 10^{-7}$
Shift in accelerator alignment - horizontal (April - August 1966) - vertical		0.5 mm (max) 1 mm (max)

[1]This number had been adjusted to take into account non-standard accelerator girders.

[2]Based on 90% availability of klystrons.

[3]The tuning range is 2856 ± 0.1 MHz.

[4]Improvements are still required to make the system more reliable.

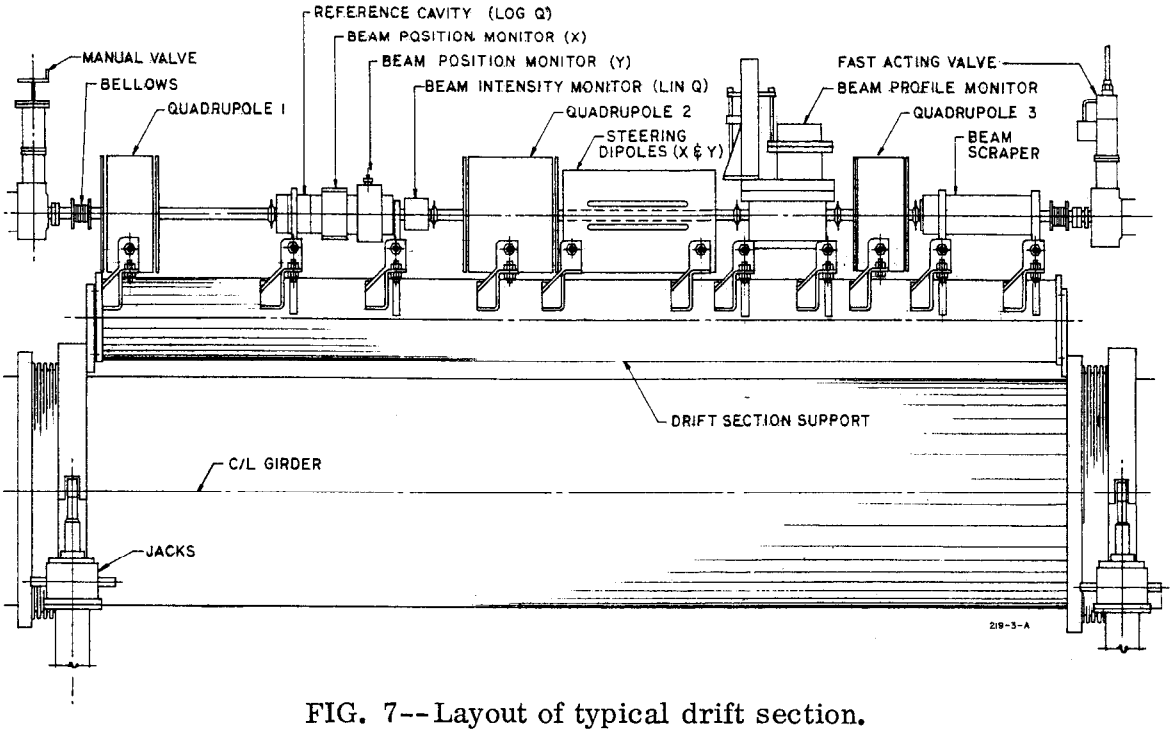

FIG. 7--Layout of typical drift section.

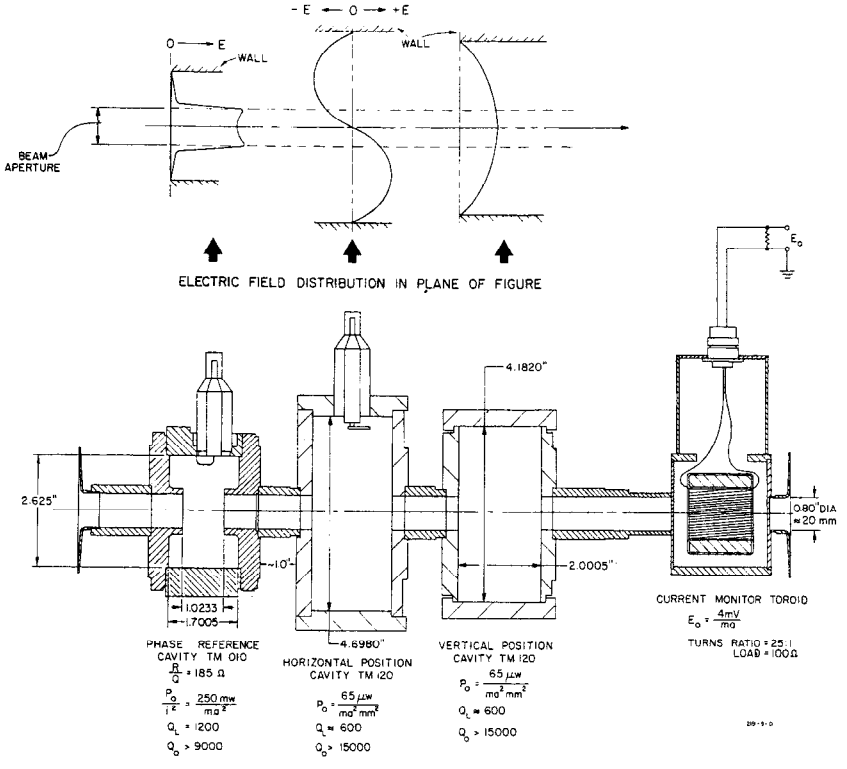

FIG. 8--Beam intensity and position monitors.

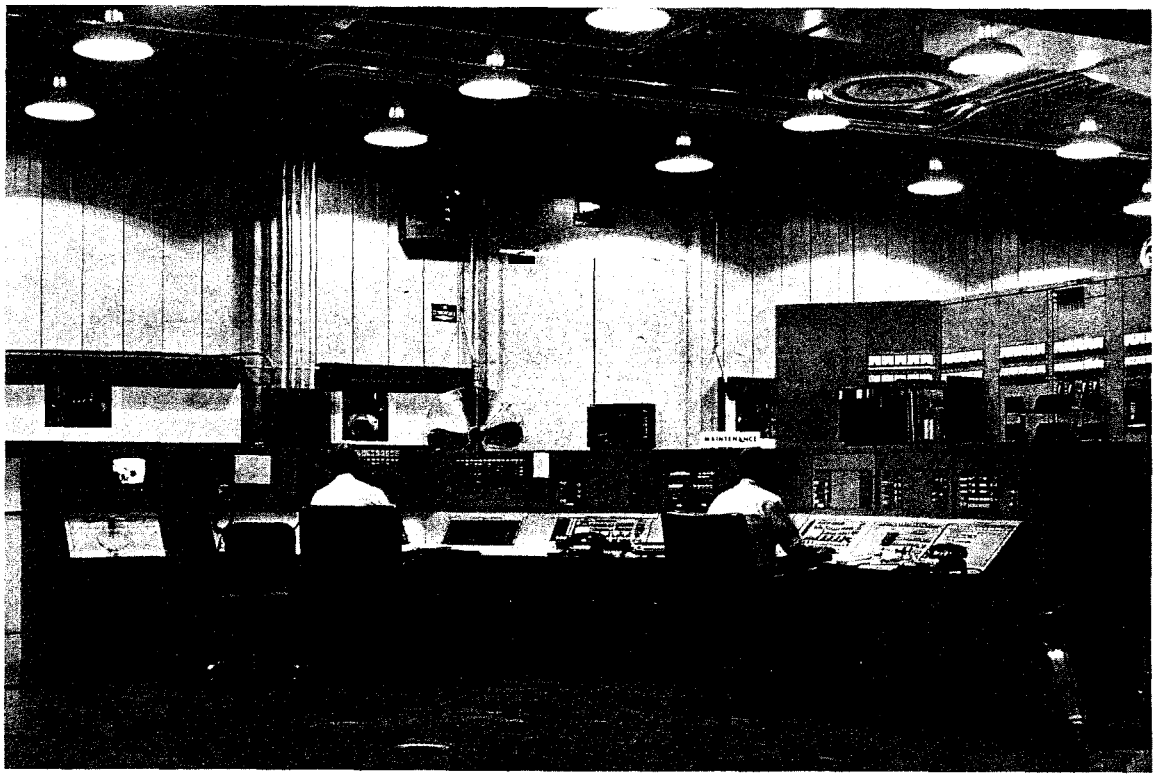

FIG. 9--The maintenance console in Central Control.

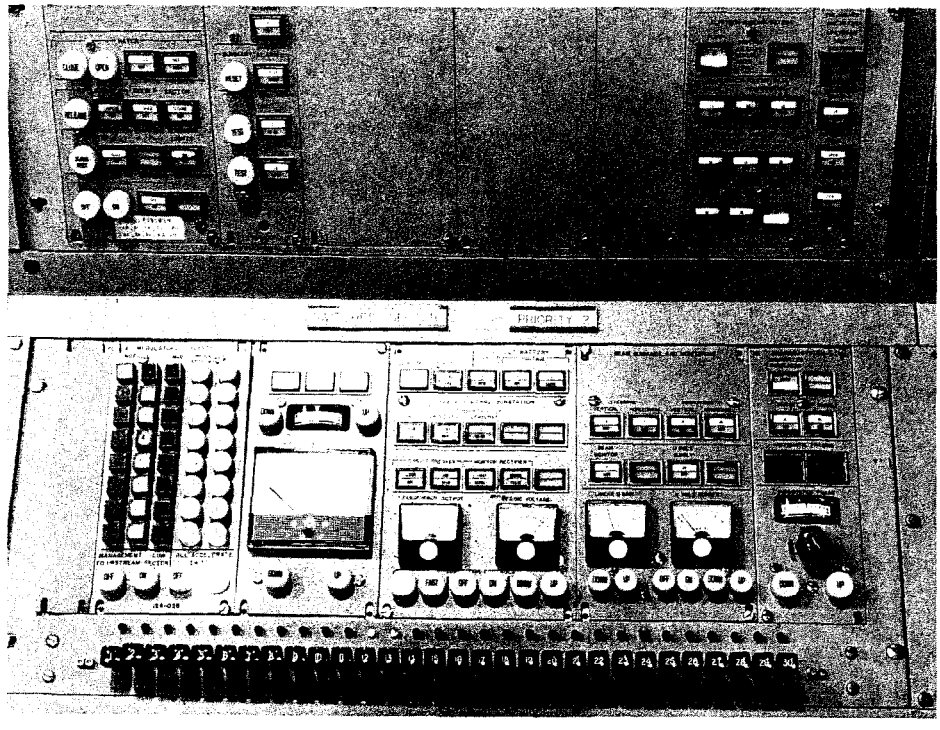

FIG. 10--Switched-sector panel in Central Control.

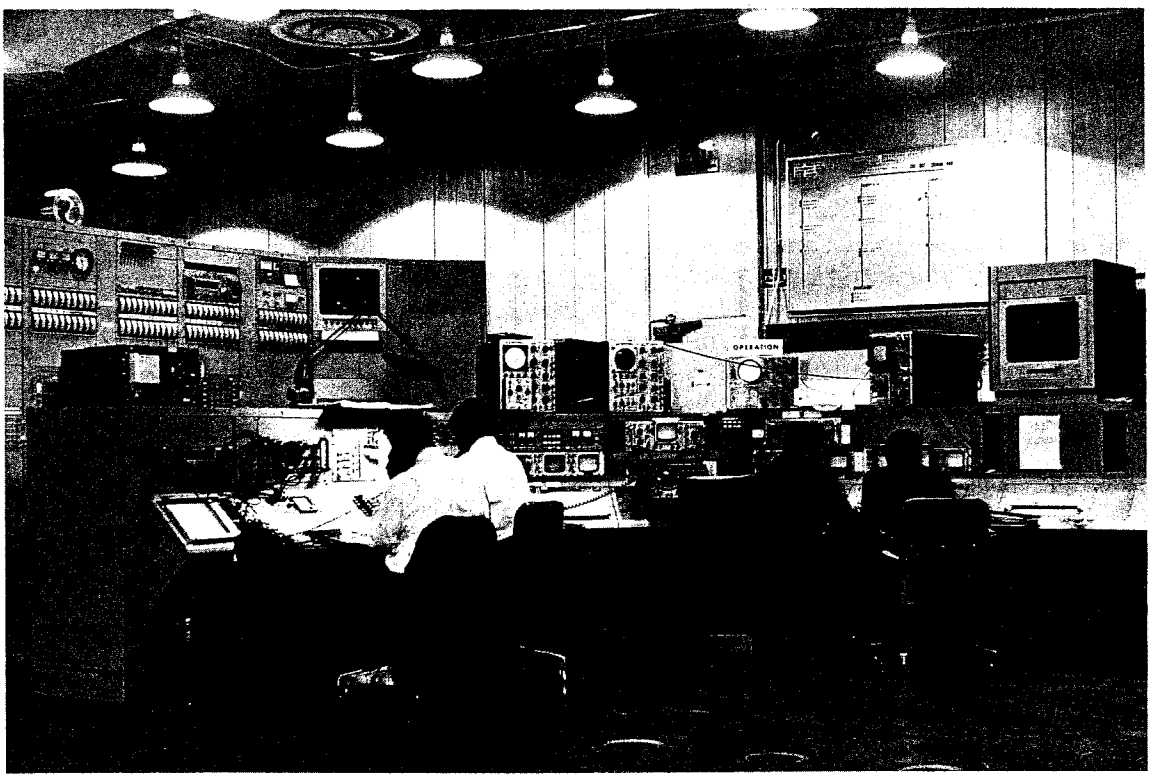

FIG. 11--The beam operator console in Central Control.

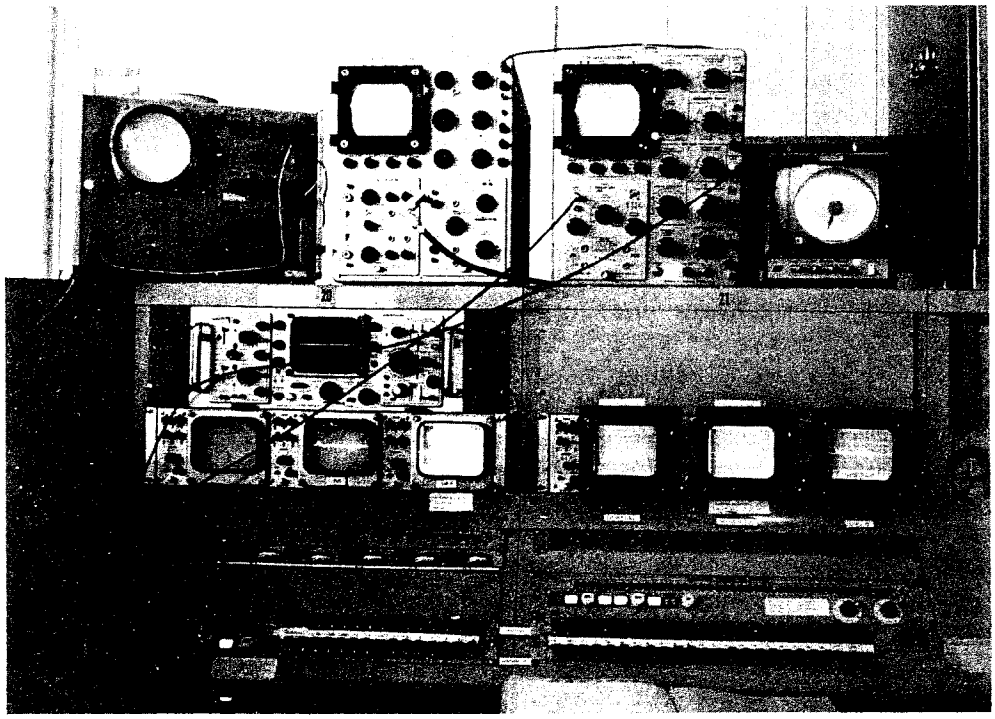

FIG. 12--Beam guidance instrumentation at Central Control.

numerous telephones and the inevitable Tektronics oscilloscopes, the beam operator focuses his attention on beam guidance and beam spectrum.

Figure 12 shows various oscilloscope displays and the controls to the 70 or so steering dipoles. Beam guidance is achieved by adjusting the dipole currents while observing the effect produced on the above displays. The second oscilloscope on the left gives a display of the ionization produced by the beam as a function of axial length in the "PLIC" system. The term "PLIC" stands for "Panofsky's Long Ion Chamber," a coaxial cable under high voltage installed under the ceiling of the accelerator housing. When the electrons strike the walls of the accelerator at a given point, the travel to the Control Room time of the break-down pulse produced in PLIC at that point gives the operator an indication of where the beam is getting lost. The third oscilloscope displays, in the form of a row of dots, the current or charge which successively passes through each toroid. Finally, the last three oscilloscopes display, in the same form, the horizontal and vertical positions of the beam and the amplitude of the signal induced in each of the microwave reference cavities. Figure 13 shows in slightly better detail how the beam operator can make use of the amplitude and location of the PLIC signal to steer and focus the beam so as to successively cause it to be transmitted with less and less loss along the two-mile distance. The final trace with very small dots on the right shows that the beam steering and focusing job is finished, at least for the time being. Figure 14 gives an early example of the display of beam intensity for two simultaneous beams of different energies. The slight ripple in the displays does not indicate the violation of any law of physics but rather, slight inaccuracies in amplifier calibration.

Turning now to the beam switchyard, Fig. 15 is a photograph of the beam switchyard control room located in the Data Assembly Building. In addition to the beam control console, various racks containing the personnel protection system, and many of the beam switchyard interlocks, visible in the foreground is the SDS-925 computer. This computer, aside from interlock scanning, readout, and checking of many analog signals, etc., is used principally for the setup of all switchyard magnet currents and slit widths so that the various switched electron beams can be correctly transmitted to the respective End Stations. The next figures show some of the instruments used in the beam switchyard. Figure 16 is a front view of the vertical adjustable jaws of the collimator with their water cooling system and vacuum envelope. Figure 17 is a schematic diagram of an insertable Cerenkov light monitor with its telescope and television camera. Figure 18 shows the first two-mile beam spot obtained on such a monitor at 6:45 a.m. on May 21, 1966. Figure 19 is a photograph of one of the adjustable spectrum analyzers located upstream of the A and B slits. This device has secondary emission monitor foils of various widths for best resolution in the center. The central gap is adjustable through retraction of the two supporting members. Spectrum displays obtained from such monitors, either of the scanned type shown in Fig. 20 or of the video or gated type, available in both Central Control and the Data Assembly Building, enable the operators to make the proper adjustments either in the accelerator or in the beam switchyard to obtain the best spectrum. Figure 21 illustrates two typical energy spectra; the dotted curve shows a rather wide spectrum due to about 5% beam loading. The continuous curve shows how beam loading can be

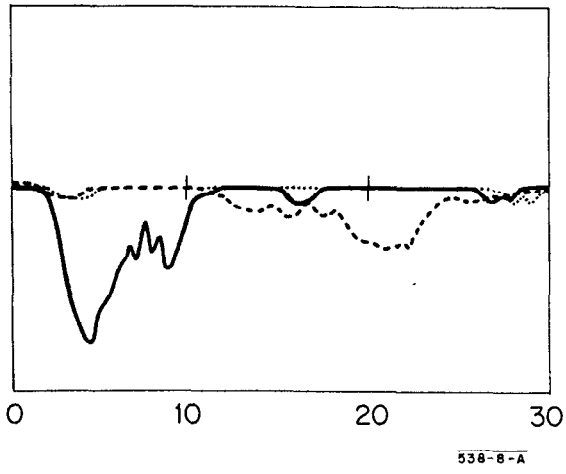

FIG. 13--Improvement of beam steering and focusing with aid of PLIC.

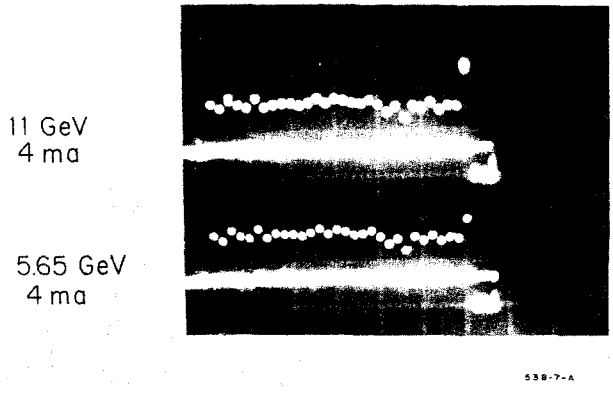

FIG. 14--Beam intensity at end of each sector for two interlaced beams.

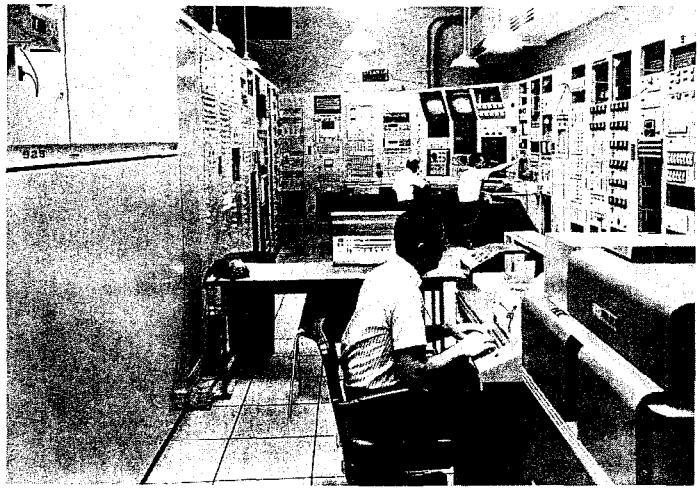

FIG. 15--Beam Switchyard Control Room.

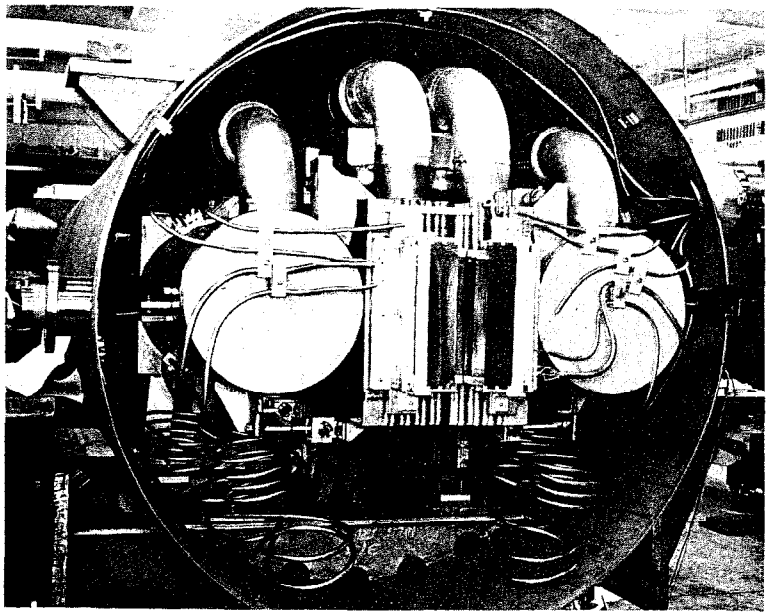

FIG. 16--Front view of collimator.

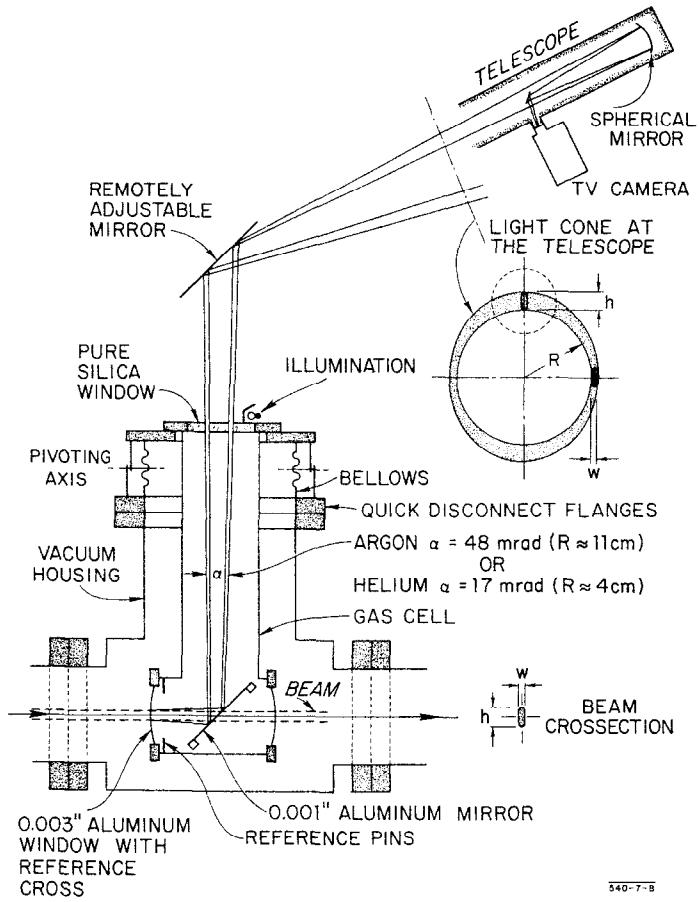

FIG. 17--Schematic diagram of insertable Cerenkov light monitor.

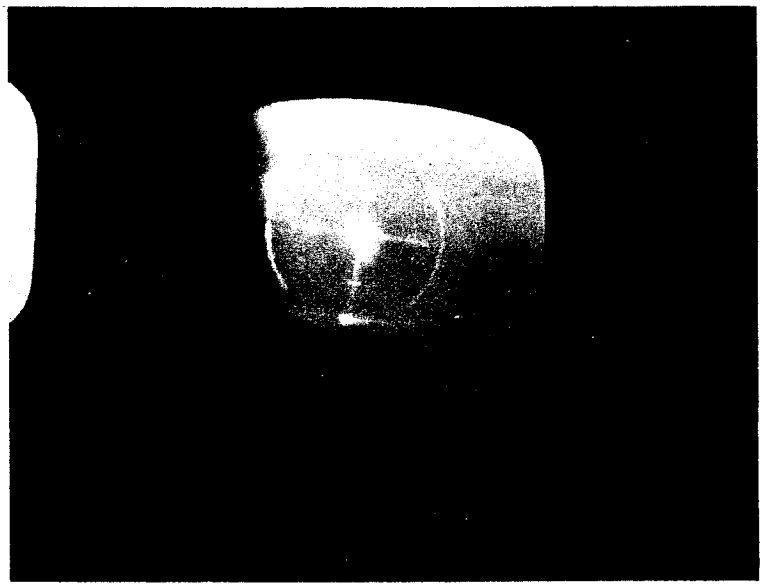

FIG. 18--View of first two-mile beam, May 21, 1966, 6:45 a.m.

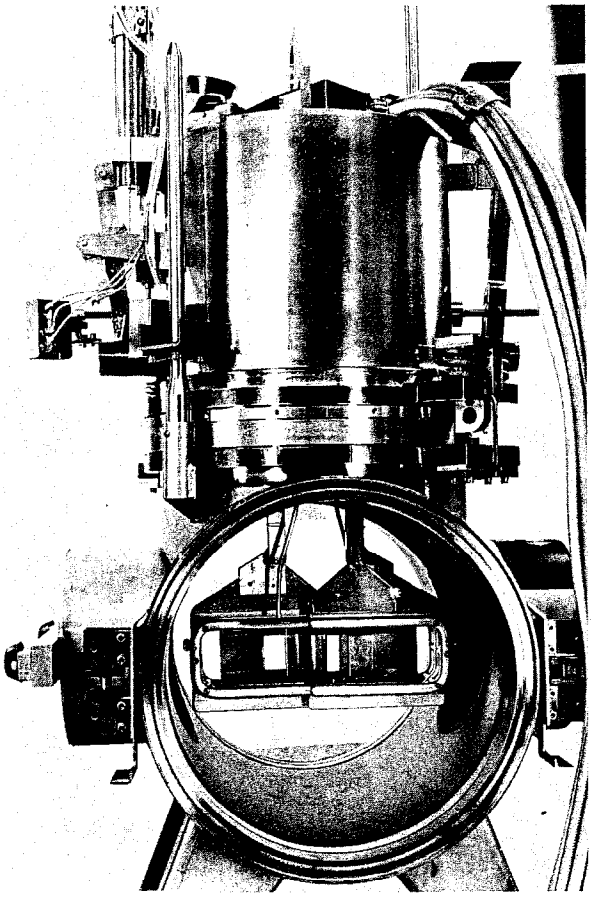

FIG. 19--Spectrum analyzer.

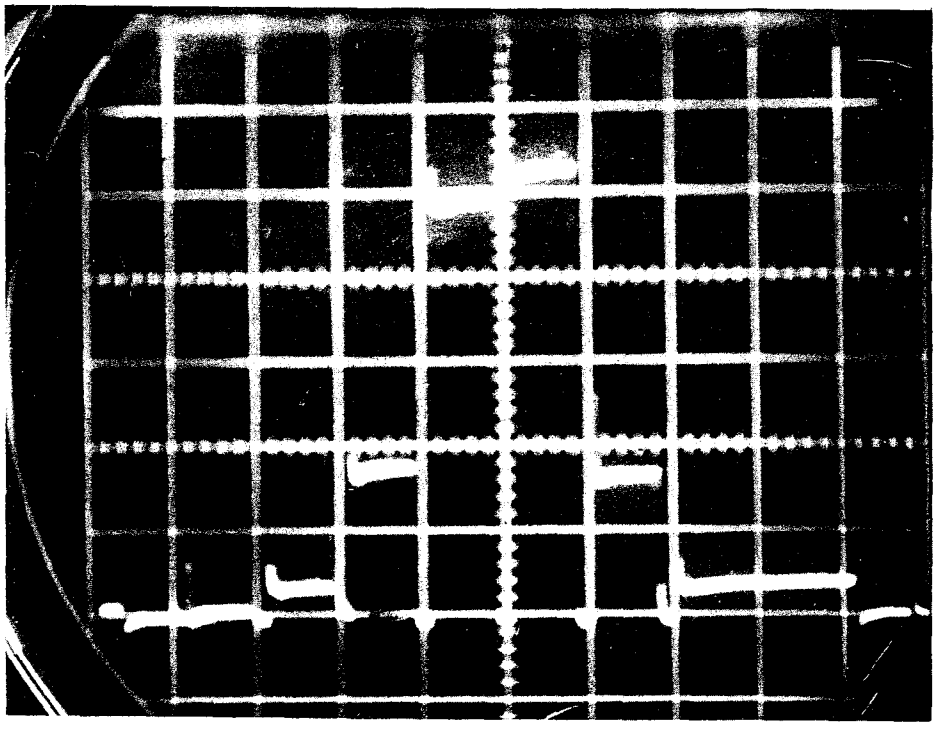

FIG. 20--Scanned spectrum display using SEM foils at tune-up dump. E = 2.5 GeV, i_p = 0.5 mA, foil width = 0.9%.

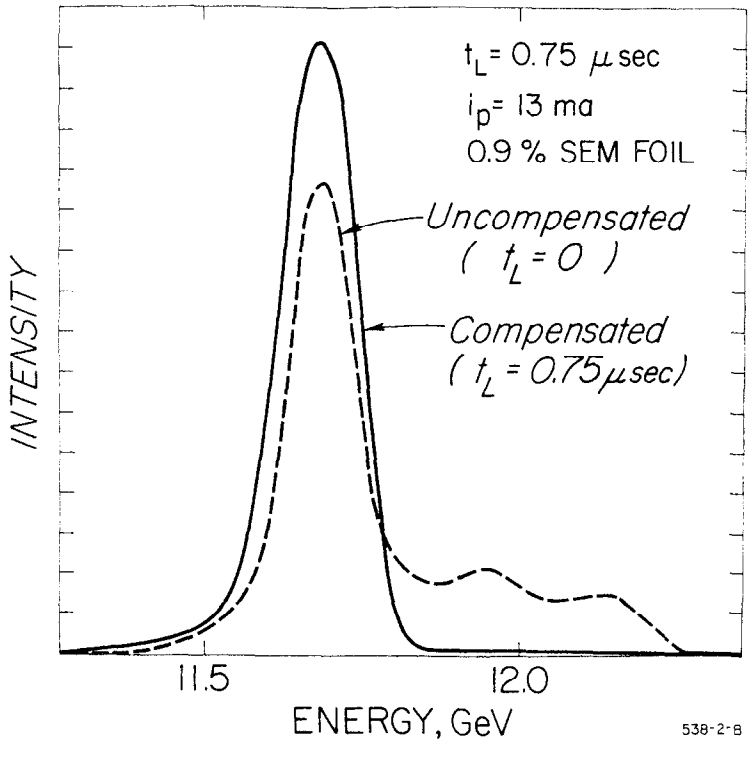

FIG. 21--Energy spectra showing effect of beam loading compensation.

compensated for by slightly delaying the triggering of a group of klystrons. Hence, the energy contribution of that particular group is added only after the initial beam loading transient has subsided. Figure 22 gives two energy spectra for two simultaneous beams, each running at 60 pps, one at 1.66 GeV, the other at 2.12 GeV. Notice that the beam intensities are identical.

As to the beam break-up phenomenon, it is hard to summarize in just a few minutes all the theoretical and experimental work which has been underway ever since the effect was discovered on the two-mile machine, shortly after beam turn-on. While the phenomenon is now fairly well understood and some of the tentative remedies are being adopted, much work remains to be done. What is clear is that the electron bunches, through initial noise or shock excitation, cause each 10-foot accelerator section to be excited in the deflecting TM_{11} mode, at a frequency of 4140 MHz. The mode is quasi-synchronous with the velocity of light and has approximately 180^{o} of phase shift per cavity. For comparison, the TM_{01} accelerating mode and the TM_{11} deflecting mode are both illustrated in Fig. 23. Asymptotically, electron bunches, on crest for maximum acceleration, set up the TM_{11} mode at a phase such that they simultaneously induce maximum field and undergo maximum deflection. This takes place at 45^{o}. As a result of cumulative interaction, both in space and in time, the latter part of the beam pulse is lost, as shown in Fig. 24. A resonant build-up takes place in the front end of each of the 960 accelerator sections, between the waveguide coupler and the seventh or eighth cavity. Beyond this point, because of the tapered constant-gradient design of the disk-loaded waveguide, the mode is cut off at this frequency.

Beam break-up seems to occur preferentially in the vertical plane, in the direction perpendicular to the input accelerator coupler. The effect is coherent within each beam pulse and cumulative, both as a function of time and length, because successive electron bunches leave behind them increasingly excited cavities whose fields impart increasing amounts of transverse momentum to the next bunches, alternately up and down. Both theory and experiment seem to indicate that for a given energy gradient and focusing condition, the product $[t\ i\ z]$, where t is the time to break-up, i is the peak current, and z is the axial position where the beam strikes the accelerator wall, is approximately constant. This relation implies that for a given length, the charge which can be transmitted through the machine is constant.

The experiments and remedies which are being considered are basically of two types: microwave suppression or feedback of the spurious mode and additional focusing. Many experiments of the microwave type have been performed, both at 4140 MHz and at harmonically related frequencies such as 4428 (= 2856 × 3 - 4140 MHz), 1284 (= 4140 - 2856 MHz) and 1572 MHz (= 4428 - 2856 MHz). For the first time, just a few days ago, we were able to recover a small fraction of the beam (otherwise broken up and lost at the end of the pulse) by abstracting the 1284-MHz signal from the beam through a microwave cavity and feeding it back through a second, neighboring cavity, after proper amplification ($\approx$80 dB) and phase shifting. However, because these microwave devices are rather costly and difficult to adjust, we are presently giving preference to a more "macroscopic" remedy which consists of strengthening the quadrupole focusing system along the machine. This remedy should increase our transmitted current by 50 percent. As mentioned earlier, our

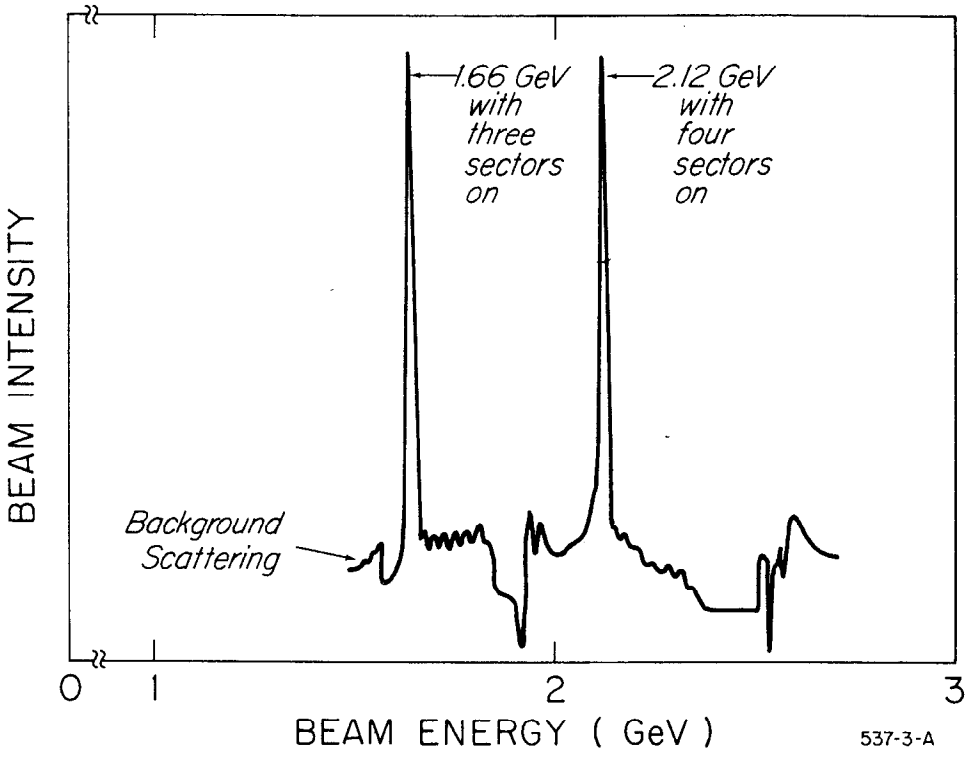

FIG. 22--Energy spectra for two simultaneous beams of different energies.

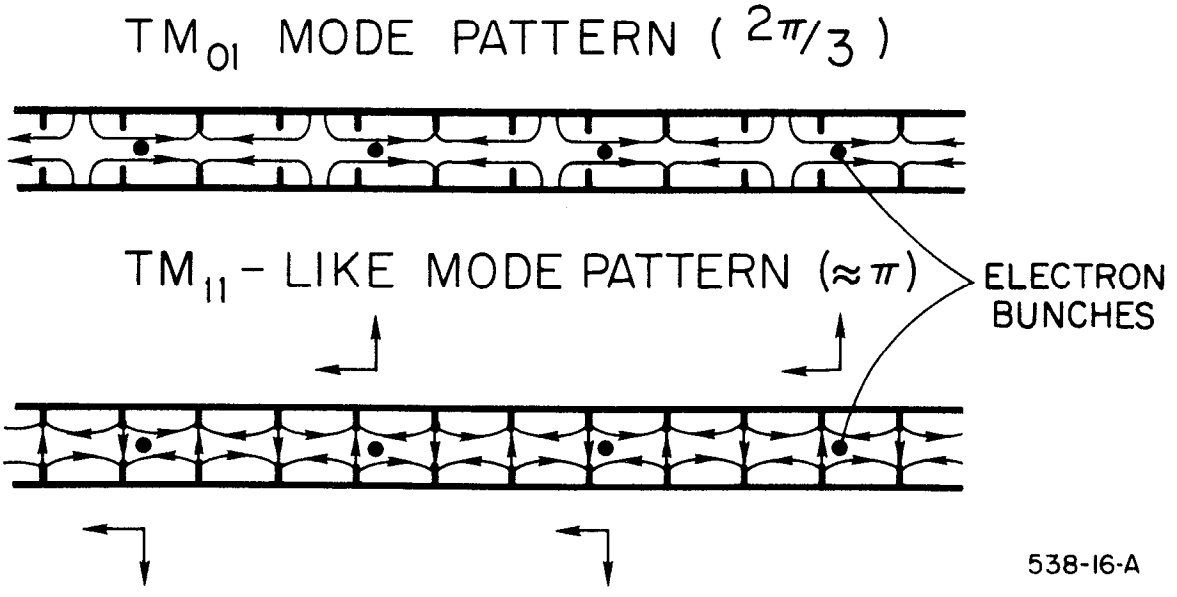

FIG. 23--TM_{01} and TM_{11} mode configurations in disk-loaded waveguide.

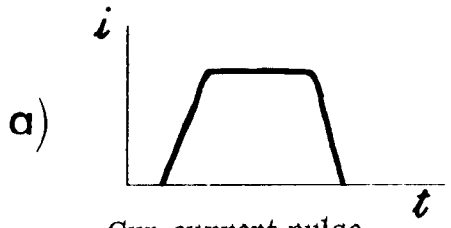

Gun current pulse.

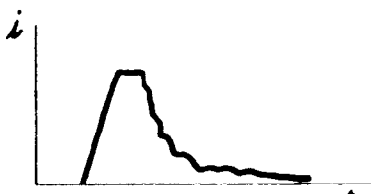

Broken-up accelerator current pulse.

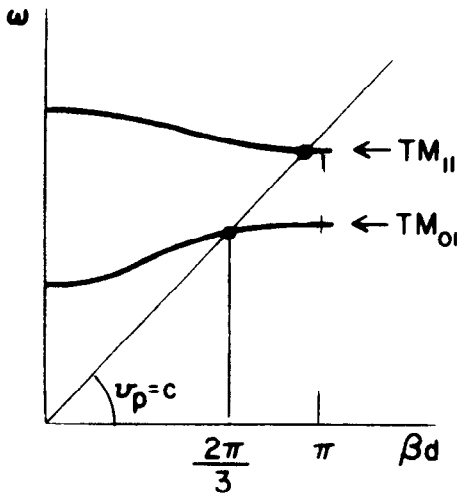

b) TM_{01} and TM_{11}-like modes for uniform or constant impedance structure.

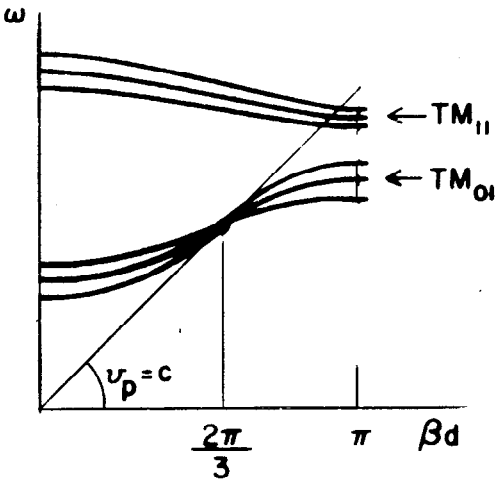

c) TM_{01} and TM_{11}-like modes for non-uniform or constant gradient structure.

538 A

FIG. 24--The beam break-up effect and the respective Brillouin diagrams for a constant impedance and a constant gradient accelerator section.

triplet system will gradually be changed into a doublet system which appears to work just as well. New doublet drift sections will be rebuilt using the left-over middle quadrupoles, which are stronger. These drift sections will be placed in the second and last third of the machine where the higher energy requires and permits stronger focusing.

After this new deployment of stronger quadrupole doublets, it will be possible to use approximately 40 of the smaller quadrupoles no longer used at the end of the machine; it is planned to install singlets between successive girders, every 40 feet, at the beginning of the machine. These closely spaced magnets will make it possible to increase the focusing of the beam at low energy without running into stop-bands. This remedy should allow us to more than double our present transmitted current and thereby meet the original specification of 50-mA peak current. Other microwave and focusing solutions are being contemplated beyond these steps to increase the current even further at a later date.

To conclude, since many of you are visiting this laboratory for the first time, I would like to present a few photographs which constitute landmarks in our overall construction effort. Figure 25 is a view of the SLAC landscape before the start of construction. Figure 26 shows the beginning of the accelerator housing construction. Next, in Fig. 27, you can see the installation of a part of the laser light pipe vacuum system. Figure 28 illustrates the installation of the collimators and Fig. 29, the arrival of a pole for the power lines, by helicopter. A view of the first klystron gallery "traffic jam" is shown in Fig. 30. Figure 31 is a photograph of a fire prevention rehersal in the beam switchyard, using a fire quenching foam generator. Figure 32 shows a panoramic view of the SLAC site taken on August 15, 1966. Finally, Fig. 33 is a photograph of a model of the strange prehistoric fossile found on the SLAC site during excavations in the End Stations: the paleoparadoxia, first Nobel Prize winner at SLAC.

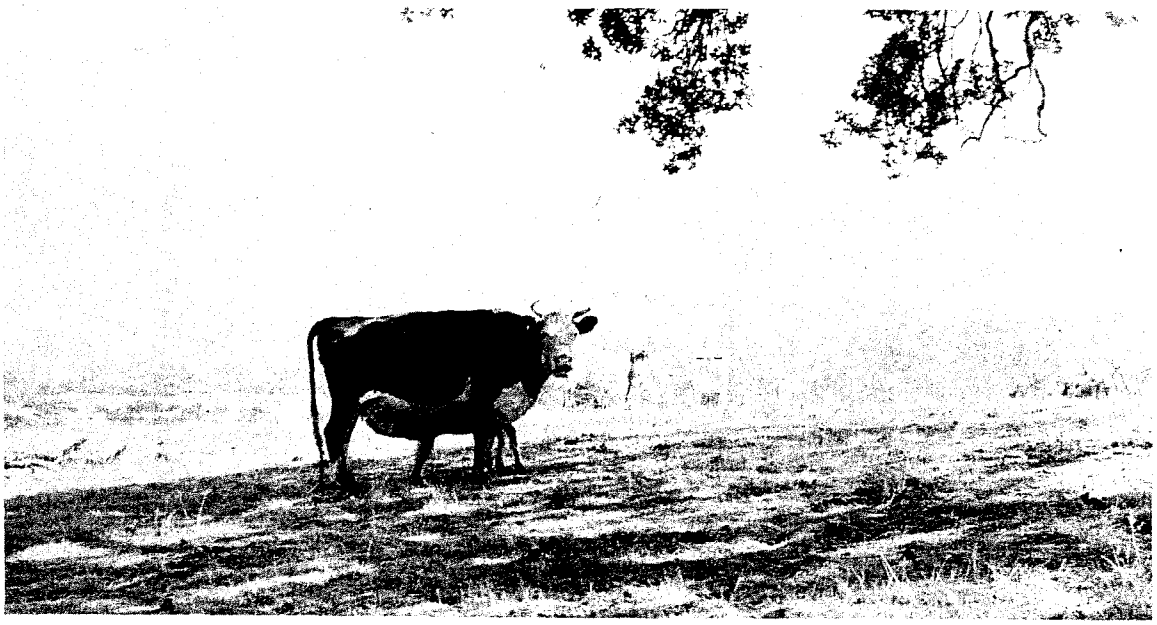

FIG. 25--The SLAC landscape in 1961, before start of construction.

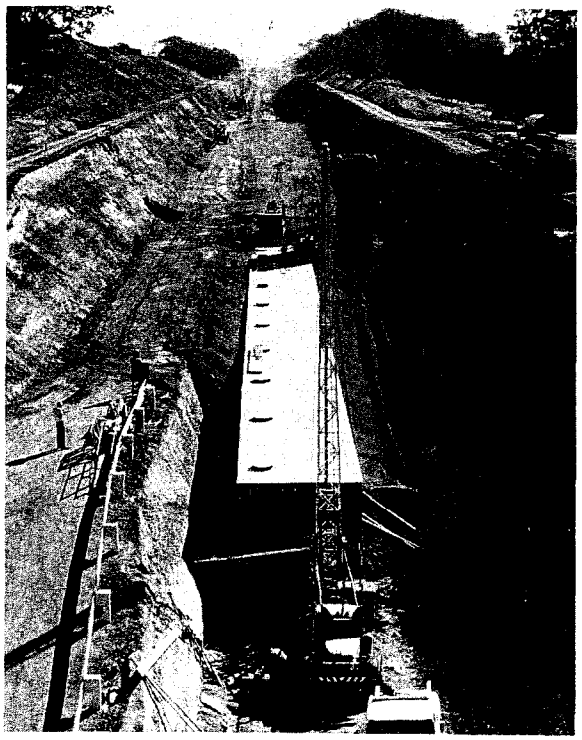

FIG. 26--The beginning of the Accelerator Housing construction.

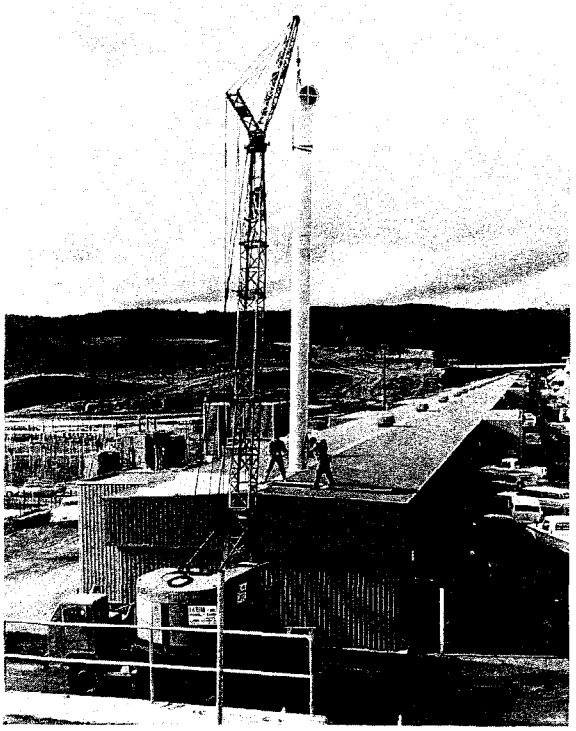

FIG. 27--Installation of a part of the laser vacuum system at the end of the Klystron Gallery.

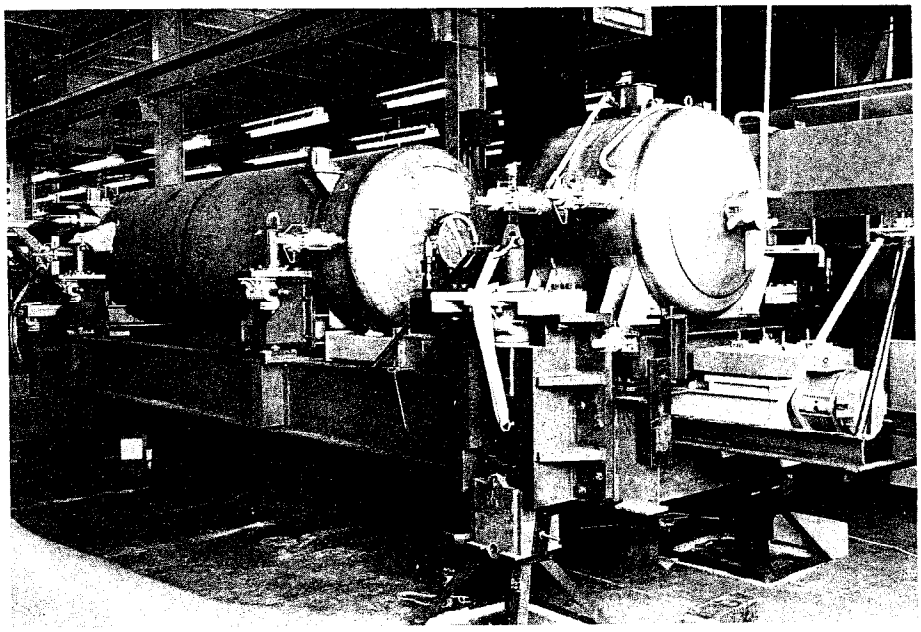

FIG. 28--Installation of the collimators.

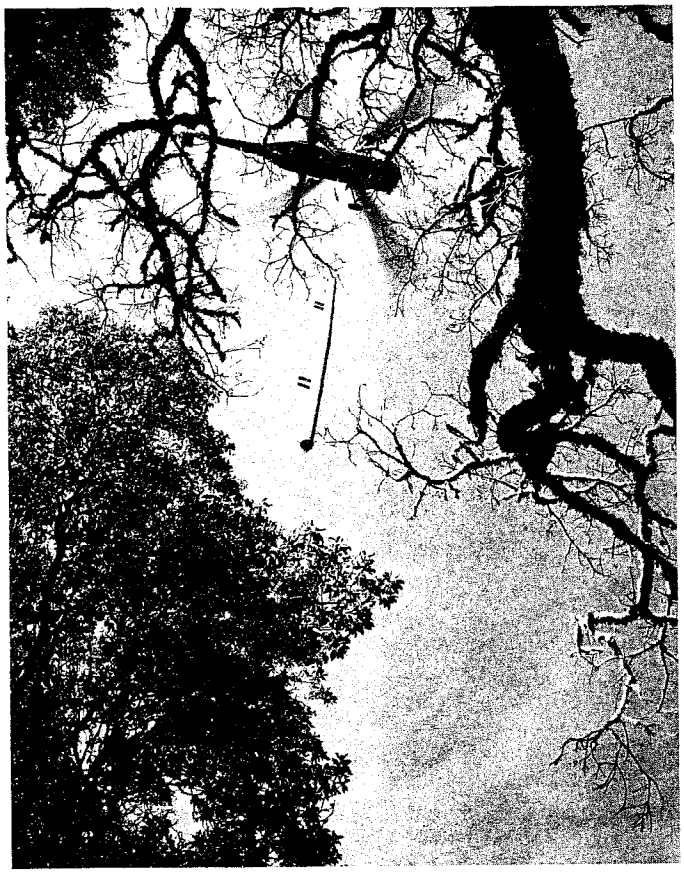

FIG. 29--Installation of a 220-kV power line pole by a helicopter.

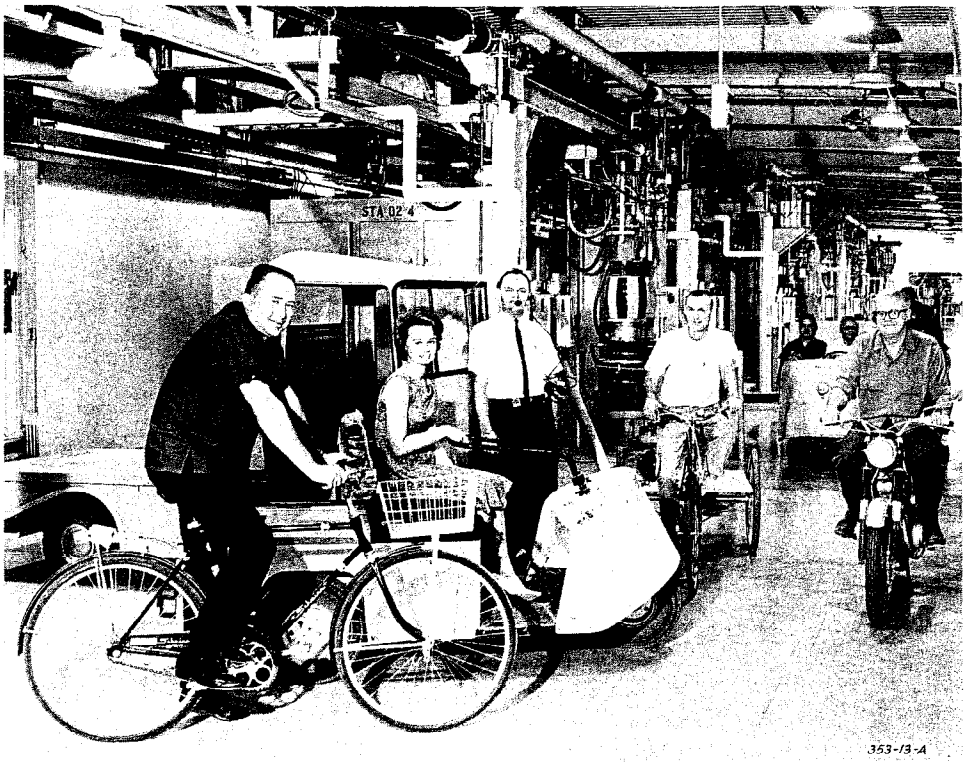

FIG. 30--Modern communications systems at SLAC or the first traffic jam in the Klystron Gallery.

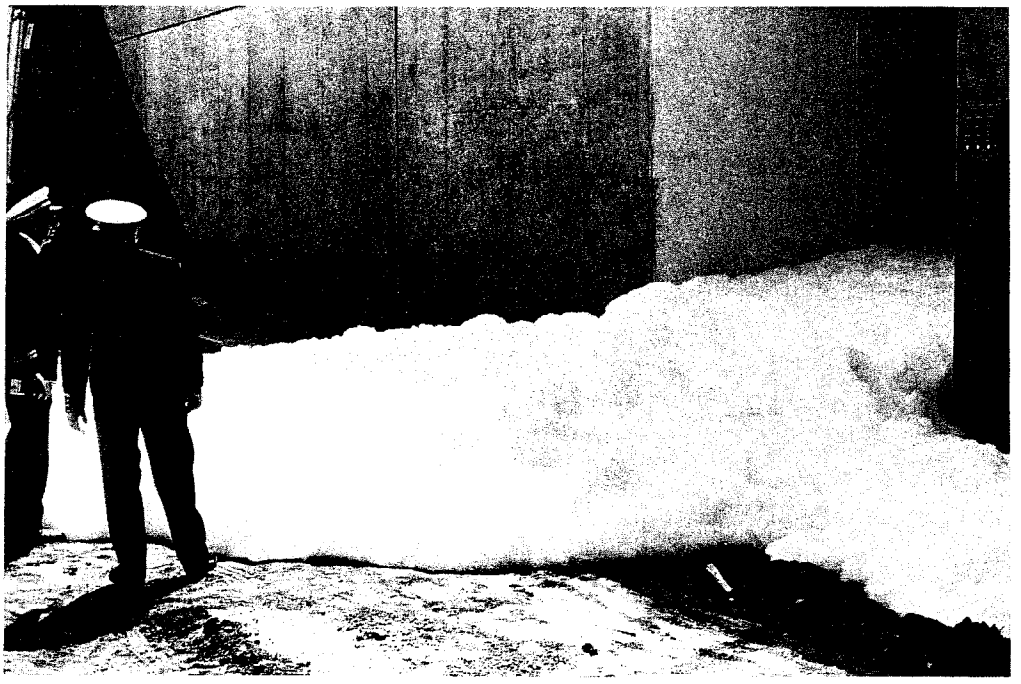

FIG. 31--A fire prevention rehearsal in the Beam Switchyard using a foam generator.

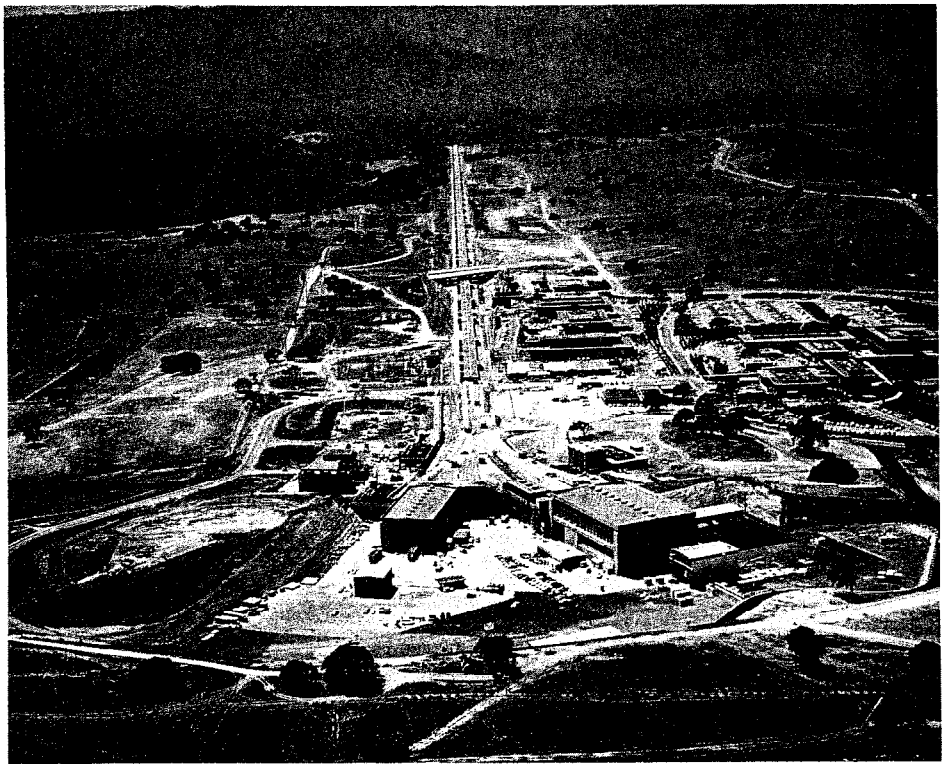

FIG. 32--Panoramic view of SLAC site, August 15, 1966.

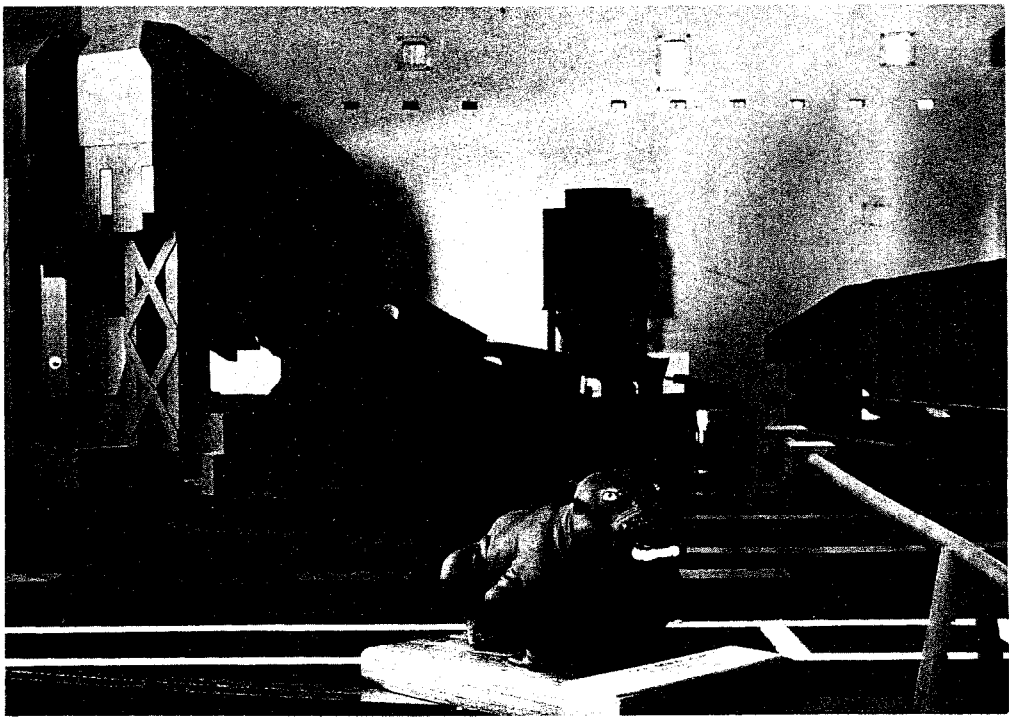

FIG. 33--The Paleoparadoxia, first Nobel Prize winner at SLAC.